

UNVEILING THE NATURE OF THE UNIDENTIFIED GAMMA-RAY SOURCES IV: THE *SWIFT* CATALOG OF POTENTIAL X-RAY COUNTERPARTS

A. PAGGI¹, F. MASSARO², R. D'ABRUSCO¹, H. A. SMITH¹, N. MASETTI³, M. GIROLETTI⁴, G. TOSTI⁵, S. FUNK²

version March 2, 2022: fm

ABSTRACT

A significant fraction ($\sim 30\%$) of the high-energy gamma-ray sources listed in the second *Fermi* LAT (2FGL) catalog are still of unknown origin, being not yet associated with counterparts at lower energies. In order to investigate the nature of these enigmatic sources, we present here an extensive search of X-ray sources lying in the positional uncertainty region of a selected sample of these Unidentified Gamma-ray Sources (UGSs) that makes use of all available observations performed by the *Swift* X-ray Telescope before March 31, 2013, available for 205 UGSs. To detect the fainter sources, we merged all the observations covering the *Fermi* LAT positional uncertainty region at 95% level of confidence of each UGSs. This yields a catalog of 357 X-ray sources, finding candidate X-ray counterparts for $\sim 70\%$ of the selected sample. In particular, 25% of the UGSs feature a single X-ray source within their positional uncertainty region while 45% have multiple X-ray sources. For each X-ray source we also looked in the corresponding *Swift* UVOT merged images for optical and ultraviolet counterparts, also performing source photometry. We found ultraviolet-optical correspondences for $\sim 70\%$ of the X-ray sources. We searched several major radio, infrared, optical and ultraviolet surveys for possible counterparts within the positional error of the sources in the X-ray catalog to obtain additional information on their nature. Applying the kernel density estimator technique to infrared colors of WISE counterparts of our X-ray sources we select 6 γ -ray blazar candidates. In addition, comparing our results with previous analyses, we select 11 additional γ -ray blazar candidates.

Subject headings: X-rays: galaxies - gamma rays: observations - galaxies: active - radiation mechanisms: non-thermal - catalogs

1. INTRODUCTION

One of the biggest challenges of modern γ -ray astronomy and one of the main scientific objectives of the ongoing *Fermi* mission is unraveling the nature of the Unidentified Gamma-ray Sources (UGSs) (e.g., [Abdo et al. 2009](#); [Atwood et al. 2009](#)).

Since the Third EGRET catalog (3EG)⁶ (e.g., [Hartman et al. 1999](#)) the fraction of γ -ray sources without an assigned counterpart at low energies has been significant $\sim 30\%$ (e.g., [Sowards-Emmerd, Romani, & Michelson 2003](#)). This situation was mostly unchanged in the revised EGRET catalog (EGR; [Casandjian & Grenier 2008](#)), even though the improved background modeling applied in the EGR resulted in fewer γ -ray detections (188 sources in total, in contrast to 271 listed in 3EG); 87 out of 188 EGR entries remain unassociated.

The UGSs at low Galactic latitude ($|b| < 10^\circ$) are expected to be associated with local objects lying in our Galaxy, such as molecular clouds (as consequence of interaction with cosmic-rays), supernova remnants, massive stars, pulsars and pulsar wind nebulae, or X-ray binaries (see, e.g., [Gehrels & Michelson 1999](#); [Casanova et al. 2010](#); [Yan, Lazarian, & Schlicke-](#)

[eiser 2012](#); [Ackermann et al. 2013](#); [Dermer & Powale 2013](#)) although there are few rare cases of γ -ray blazars detected through the Galactic plane (e.g. *Fermi* J0109+6134, see [Vandenbroucke et al. 2010](#)). On the other hand, the population of UGSs above the Galactic plane is generally believed to be dominated by extragalactic sources, although there is a suspected Galactic component as well (e.g., [Oezel & Thompson 1996](#); [Mirabal et al. 2000](#); [Reimer 2001](#); [Nolan et al. 2012](#)). According to one of the most recent *Fermi* discoveries, several millisecond pulsars have been found at high Galactic latitudes ([Abdo et al. 2010a,b](#); [Nolan et al. 2012](#)).

A large fraction of these UGSs could be blazars, the rarest class of radio-loud active galactic nuclei, whose emission dominates the gamma-ray sky (e.g., [Mukherjee et al. 1997](#); [Abdo et al. 2010c](#)). Their observational properties are generally interpreted in terms of a relativistic jet aligned within a small angle to our line of sight ([Blandford & Rees 1978](#)).

The blazar spectral energy distributions (SEDs) typically show two peaks. The first one, lying in the range of radio - soft X-rays, is widely held to be due to synchrotron emission by highly relativistic electrons within their jet. The second one lies at hard X-ray or γ -ray energies, and is interpreted as inverse Compton upscattering by the same electrons of the seed photons provided by the synchrotron emission ([Inoue & Takahara 1996](#); [Finke, Dermer, Böttcher 2008](#)) with the possible addition of seed photons from outside the jets yielding contributions to the non-thermal radiations due to external inverse Compton scattering (see [Dermer & Schlickeiser 1993, 2002](#); [Dermer et al. 2009](#); [Finke 2013](#)) often dominating their γ -ray outputs ([Ackermann et al. 2011](#)).

Blazars are also known X-ray sources since *ROSAT* DXRBs ([Perlman et al. 1998](#); [Landt et al. 2001](#)) and *Einstein* IPC ([Elvis et al. 1992](#); [Perlman, Schachter, & Stocke 1999](#)) sur-

¹ Harvard - Smithsonian Astrophysical Observatory, 60 Garden Street, Cambridge, MA 02138, USA

² SLAC National Laboratory and Kavli Institute for Particle Astrophysics and Cosmology, 2575 Sand Hill Road, Menlo Park, CA 94025, USA

³ INAF - Istituto di Astrofisica Spaziale e Fisica Cosmica di Bologna, via Gobetti 101, 40129, Bologna, Italy

⁴ INAF Istituto di Radioastronomia, via Gobetti 101, 40129, Bologna, Italy

⁵ Dipartimento di Fisica, Università degli Studi di Perugia, 06123 Perugia, Italy

⁶ <http://heasarc.gsfc.nasa.gov/W3Browse/cgrog/egret3.html>

veys (see also [Perlman 2000](#)). Since then, the X-ray properties of blazars have been deeply investigated by many authors (see for example [Giommi & Padovani 1994](#); [Padovani & Giommi 1995](#); [Massaro et al. 2011b](#); [Massaro, Paggi, & Cavaliere 2011c](#)). [Massaro et al. \(2008a\)](#) in particular studied *Swift* observations of a sample of low and intermediate peaked BL Lacs, for which the X-ray emission is expected to lie in the “valley” between the low and high energy spectral components, finding these sources to be bright in the X-ray with fluxes above $\sim 10^{-13}$ erg cm $^{-2}$ s $^{-1}$. In addition we note that $\sim 75\%$ of the γ -ray blazars listed in the Second LAT AGN Catalog (2LAC, [Ackermann et al. 2011](#)) are also X-ray sources with fluxes above $\sim 10^{-14}$ erg cm $^{-2}$ s $^{-1}$.

However, due to the incompleteness of the current radio and X-ray surveys used for the gamma-ray associations, it is not always possible to identify a blazar-like counterpart to a UGS⁷.

Radio follow up observations of UGSs have been performed or are still in progress (e.g., [Kovalev 2009a](#); [Kovalev et al. 2009b](#); [Mahony et al. 2010](#); [Petrov et al. 2013](#)). [Massaro et al. \(2013b\)](#) recently proposed a method for searching γ -ray blazar-like candidate counterparts of the UGSs based on the combination of radio observations from Westerbork Northern Sky Survey (WENSS; [Rengelink et al. 1997](#)), those of the NRAO Very Large Array Sky survey (NVSS; [Condon et al. 1998](#)) and the Very Large Array Faint Images of the Radio Sky at Twenty-Centimeters (FIRST, [Becker, White, & Helfand 1995](#); [White et al. 1997](#)).

In addition, a procedure to recognize blazar-like candidate counterparts for UGSs on the basis of their infrared (IR) colors have been successfully implemented by [D’Abrusco et al. \(2012, 2013\)](#) and [Massaro et al. \(2012a, 2013a\)](#) making use of the Wide-Field Infrared Survey Explorer (WISE) all-sky data ([Cutri et al. 2012a](#)). WISE data also proven to be useful to address the widely entertained field of mid-infrared AGN selection ([Stern et al. 2005, 2012](#), see also [Eckart et al. 2010](#); [Park et al. 2010](#)).

Additional attempts have been recently developed to associate or to characterize the UGSs using pointed *Swift* observations (e.g., [Mirabal 2009](#); [Mirabal & Halpern 2009](#); [Kataoka et al. 2012](#)), and/or with several statistical approaches (e.g., [Mirabal, Nieto, & Pardo 2010](#); [Ackermann et al. 2012](#)). Moreover, in the last two years the *Chandra* and *Suzaku* X-ray telescopes have been used to investigate the nature of the UGSs (e.g., [Fujinaga et al. 2011](#); [Maeda et al. 2011](#); [Murakami et al. 2011](#); [Cheung et al. 2012](#); [Mori et al. 2012](#)).

The characterization of X-ray emission from UGSs is of particular interest. All γ -ray sources associated in the second *Fermi* LAT (2FGL) catalog have a clear radio counterpart ([Nolan et al. 2012](#)) leading to the so called radio- γ -ray connection in the case of blazars (e.g., [Ghirlanda et al. 2010](#); [Ackermann et al. 2011](#); [Massaro et al. 2013b](#)). However this is not the case for the X-ray sources. It is not clear at the moment if all γ -ray sources feature an X-ray counterpart and therefore a systematic study of X-ray emission from UGS is useful to investigate their nature.

Motivated by these researches, we investigate the X-ray- γ connection presenting in this paper a catalog of X-ray sources lying in the positional uncertainty region of all UGSs listed

⁷ We note that, in the following, we will refer to a source lying into the positional uncertainty region of a γ -ray source as “candidate counterpart”, while we will use the term “blazar candidate” for the γ -ray source together with its unique blazar-like counterpart.

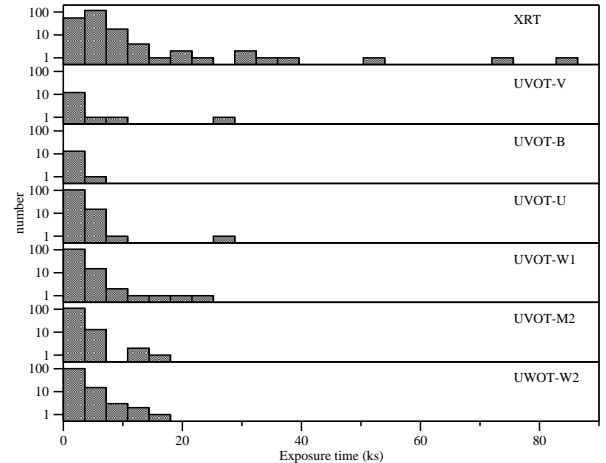


Figure 1. Histograms of total exposures of the merged observations discussed in Section 2.

in 2FGL without any γ -ray analysis flag, making use of all available observations performed by *Swift* X-ray Telescope (XRT) up to March 31, 2013, and we investigate their multi-wavelength properties.

For X-ray sources with a WISE counterpart we then apply the Kernel Density Estimation (KDE) technique to compare their IR colors to those of known γ -ray blazars, selecting 44 new blazar-like candidate counterparts and 6 γ -ray blazars candidates as a result.

The paper is organized as follows: Section 2 is devoted to the UGS sample definition while Section 3 describes the main data reduction procedure adopted for the *Swift* XRT and *Swift* UVOT observations. The complete list of X-ray sources that could be potential counterpart of UGSs in the 2FGL catalog is presented in Section 4. In Section 5 we illustrate our selection of new γ -ray blazar candidates. In Section 6 we compare our results with different, previous selections, and Section 7 is dedicated to our conclusions.

2. SAMPLE SELECTION

The initial sample considered in our analysis is constituted by the 299 UGSs in the 2FGL catalog that do not present any γ -ray analysis flag⁸ ([Nolan et al. 2012](#)).

Up to March 31, 2013, 205 of these sources feature at least one X-ray observation in the *Swift* master catalog⁹ performed in photon counting (PC) mode, and covering the positional uncertainty region at 95% level of confidence as reported in the 2FGL. The final sample considered in this analysis is therefore constituted by the above selected 205 sources.

The *Swift* observations have variable exposures, and to detect the fainter X-ray objects we merged all the observations corresponding to each UGSs (see Section 3 for details on the reduction procedures), obtaining the total exposures shown in Figure 1.

3. SWIFT OBSERVATIONS AND DATA REDUCTION PROCEDURES

Swift has proven to be an excellent multi-frequency observatory for blazar research, so far observing hundreds of sources (e.g., [Moretti et al. 2007, 2012](#); [Dai, Bregman, &](#)

⁸ Analysis flags in 2FGL identify a number of conditions that can shed doubt on a source, and they are described in detail in Table 3 of [Nolan et al. \(2012\)](#).

⁹ <http://heasarc.gsfc.nasa.gov/W3Browse/all/swiftmastr.html>

Kochanek 2012) and yielding an extremely rich and unique database of multi-frequency (optical, UV, X-ray), simultaneous blazar observations. Several papers on samples selected with different criteria have already been published, including: blazars detected at TeV energies (e.g., Massaro et al. 2008b, 2011a,b; Massaro, Paggi, & Cavaliere 2011c), simultaneous optical-to-X-ray observations of flaring TeV sources (e.g., Perri et al. 2007; Tramacere et al. 2007) as well as the investigation of low and high frequency peaked BL Lacs (e.g., Maselli et al. 2010; Giommi et al. 2012). *Swift* has also been used for UV-optical and X-ray follow-up observations of TeV flaring blazars (e.g., Aliu et al. 2011; Aleksić et al. 2012; H.E.S.S. Collaboration et al. 2013) and has also been useful in obtaining photometric redshift constraints for many *Fermi*-detected BL Lacs (Rau et al. 2012).

Once *Fermi* was launched, the *Swift* XRT Survey of *Fermi* Unassociated Sources was started to perform follow-up observations of the UGSs in an attempt to find their potential X-ray counterparts¹⁰ (PI A. Falcone). In the following sections we analyze all the data collected between the beginning of the follow-up program until March 31, 2013, for the selected sample of UGSs described in Section 2.

During these observations, *Swift* operated with all its instruments in data taking mode. For our analysis, however, we consider only *Swift* XRT (Burrows et al. 2005) and *Swift* UVOT (Roming et al. 2005) data.

3.1. *Swift* XRT data reduction

The XRT data were processed using the XRTDAS software (Capalbi et al. 2005) developed at the ASI Science Data Center and included in the HEASoft package (v. 6.13) distributed by HEASARC. For each observation of the sample, calibrated and cleaned PC mode event files were produced with the XRTPIPELINE task (ver. 0.12.6), producing exposure maps for each observation. In addition to the screening criteria used by the standard pipeline processing, we applied a further filter to screen background spikes that can occur when the angle between the pointing direction of the satellite and the bright Earth limb is low. In order to eliminate this so called bright Earth effect, due to the scattered optical light that usually occurs towards the beginning or the end of each orbit, we used the procedure proposed by Puccetti et al. (2011) and D’Elia et al. (2013). We monitored the count rate on the CCD border and, through the XSELECT package, we excluded time intervals when the count rate in this region exceeded 40 counts/s; moreover, we selected only time intervals with CCD temperatures less than -50°C (instead of the standard limit of -47°C) since contamination by dark current and hot pixels, which increase the low energy background, is strongly temperature dependent (D’Elia et al. 2013).

We then proceeded to merge cleaned event files obtained with this procedure using XSELECT, considering only observations with telescope aim point falling in a circular region of $12'$ radius centered in the median of the individual aim points, in order to have a uniform exposure. The corresponding merged exposure maps were then generated by summing the exposure maps of the individual observations with XIMAGE (ver. 4.5.1).

3.2. *Swift* XRT source detection

To detect X-ray sources in the merged XRT images, we made use of the XIMAGE detection algorithm DETECT, which lo-

cate the point sources using a sliding-cell method. The average background intensity is estimated in several small square boxes uniformly located within the image. The position and intensity of each detected source are calculated in a box whose size maximizes the signal-to-noise ratio. The net counts are corrected for dead times and vignetting using the appropriate exposure maps, and for the fraction of source counts that fall outside the box where the net counts are estimated, using the PSF calibration. Count rate statistical and systematic uncertainties are added quadratically. The algorithm was set to work in bright mode, which is recommended for crowded fields and fields containing bright sources, since it can reconstruct the centroids of very nearby sources.

We also evaluated the net count rates for the detected sources with the SOSTA algorithm that, besides the net count rates and the respective uncertainties, yields the statistical significance of each source. We note that the uncertainties in the count rates returned by SOSTA are purely statistical - i.e. do not include systematic errors - and are in general smaller than those given by DETECT. SOSTA also yields slightly different count rates from DETECT, which are in most cases more accurate, because DETECT uses a global background for the entire image, whereas SOSTA uses a local background. Thus we report both values in our analysis.

The catalog was then cleaned from spurious sources - usually occurring at count rates higher than 0.2 ph s^{-1} - by visual inspection of all the observations. Finally, we refined the source position and relative positional errors by the task XRTCENTROID of the XRTDAS package, and considered only sources falling in a circular region of radius equal to the semi-major axis of the ellipse corresponding to the positional uncertainty region of the *Fermi* source at 95% level of confidence and centered at the 2FGL position of the γ -ray source (consistently with Massaro et al. 2013a). The source designation we adopt for a source with RA HH:MM:SS.s and DEC \pm DD:MM:SS is SWXRTJHHMMSS.s \pm DDMMSS, as per D’Elia et al. (2013). The results of the detection process are presented in Appendix A in Table 1.

3.3. *Swift* UVOT observations

We note that 203 out of the 205 UGSs that constitute our sample have been also observed in the optical and UV by UVOT. We then produced for each X-ray observation the corresponding merged UVOT event files adopting standard procedures¹¹. After checking the correct WCS alignment of our images with USNO-B Catalog (Monet et al. 2003), we merged them with FAPPEND (part of FTOOLS package ver. 6.13) and then merged the images with UVOTIMSUM; the same procedure was applied to produce merged exposure maps.

For each X-ray source found with the procedure described in 3.2, we looked in the corresponding UVOT images for UV-optical counterparts falling in the relative XRT positional error. We performed source photometry using the UVOTSOURCE task using the appropriate exposure map. We adopted an aperture radius of $5''$, independently of the image filter, and took the background region in the form of circle with typical radius of $20''$ in a source-free region of the sky (e.g., Maselli et al. 2013).

As a comparison we also evaluated source photometry with the UVOTDETECT task, which detects sources in UVOT images and extracts their count rates evaluating the background level. In general, we note that although the UVOTSOURCE task yields

¹⁰ <http://www.swift.psu.edu/unassociated/>

¹¹ <http://www.swift.ac.uk/analysis/uvot/image.php>

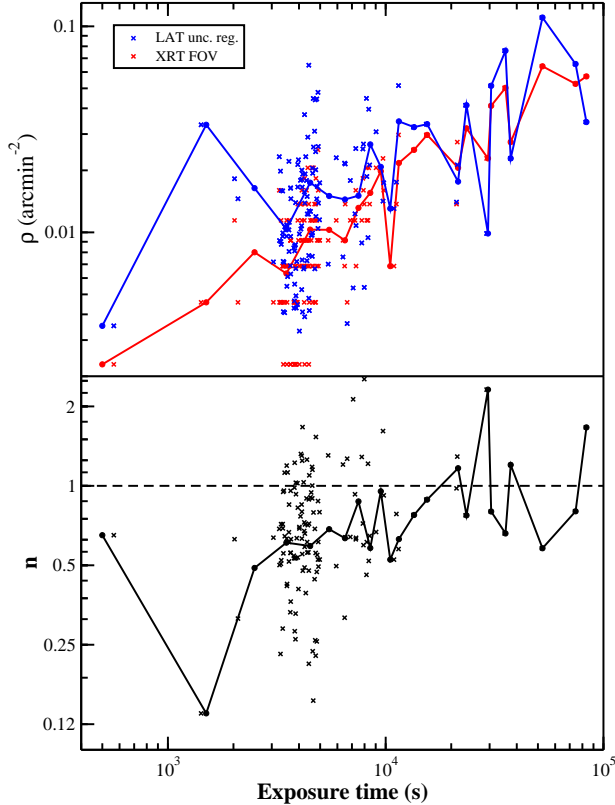


Figure 2. (Upper panel) Mean spatial density ρ of X-ray sources detected inside the LAT positional uncertainty region (blue crosses) and in the whole *Swift* XRT field of view (red crosses), as a function of the exposure time. With circles of the appropriate color we represent the average values of ρ in bins of exposure time of 1 ks. (Lower panel) Ratio n of mean spatial density of X-ray sources detected in the whole *Swift* XRT field of view to mean spatial density of X-ray sources detected inside the LAT positional uncertainty region, as a function of the exposure time (black crosses). With black circles we represent the average values of n in bins of exposure time of 1 ks.

more accurate results for extended sources, we expect to deal mostly with point-like sources. The results of the detection process are presented in Table 2.

3.4. Chance coincidence probability

Due to considerable size of the *Fermi* LAT positional uncertainty region (ranging from $\sim 2'$ to $\sim 20'$ with an average size $\sim 8'$) several UGSs feature more than one X-ray source in their uncertainty region. For this reason, we performed for each UGS listed in Table 1 simulations to evaluate the probability of chance coincidence detections of X-ray sources.

As a first step we evaluated the mean spatial density ρ of X-ray sources detected in the whole *Swift* XRT field of view and inside the LAT positional uncertainty region. In the upper panel of Figure 2 we present with red and blue crosses respectively these two densities as a function of the exposure time, while in the lower panel of the same figure we show with black crosses the ratio n of these two densities. Despite the spread, the average values of these quantities evaluated in bins of 1 ks (indicated with circles of the appropriate color) show that for exposure times higher than ~ 20 ks the two mean densities become comparable.

The mean spatial densities, however, cannot be used to properly evaluate the chance coincidence probability, since they do not take into account the spatial distribution of the X-

ray sources, that is not uniform. In order to properly evaluate the chance coincidence probability we adopted a method similar to that presented by D'Abrusco et al. (2013), that consists in randomly shifting the searching region (in our case, the LAT positional uncertainty region) and evaluate how many X-ray sources fall into this shifted region. For each UGS listed in Table 1 we generated 50 random regions of the same size of the relative LAT positional uncertainty region (and disconnected from the latter) in order to cover the whole *Swift* XRT field of view. We then counted how many of these random regions contain a number of X-ray sources equal or higher than the number of X-ray sources contained inside the LAT positional uncertainty region, evaluating for each UGS the relative chance coincidence probability that, as shown in Figure 2, depends on the source exposure. We then evaluated the average chance coincidence probability for all our UGS, that is $\sim 5\%$ with a standard deviation of $\sim 13\%$; we can therefore conservatively evaluate a chance coincidence probability $\lesssim 18\%$. This value makes us confident in associating the detected X-ray sources with the UGSs.

4. THE X-RAY CATALOG OF CANDIDATE COUNTERPARTS FOR THE UNIDENTIFIED GAMMA-RAY SOURCES

Using the procedure described in 3.2, we obtained a catalog of 357 X-ray sources detected with a significance $\geq 2\sigma$. In particular, we have 195 sources detected with a significance $\geq 3\sigma$, 111 sources with a significance $\geq 4\sigma$ and 80 sources with a significance $\geq 5\sigma$. We found X-ray sources consistent with the locations of 143 UGSs, with 51 UGSs having a single X-ray source and 92 UGSs having multiple X-ray sources in their positional uncertainty region. The remaining 62 UGSs, although overlapping with XRT-PC observations, do not show any X-ray counterpart.

In Figure 3 we show for each X-ray source of our catalog the estimated X-ray flux evaluated with PIMMS¹² 4.6b software for a standard powerlaw spectra with spectral index 2 and an absorption column density fixed to $5 \times 10^{20} \text{ cm}^{-2}$. Figure 3 clearly shows the flux limit for an X-ray source to be detected with a specific exposure.

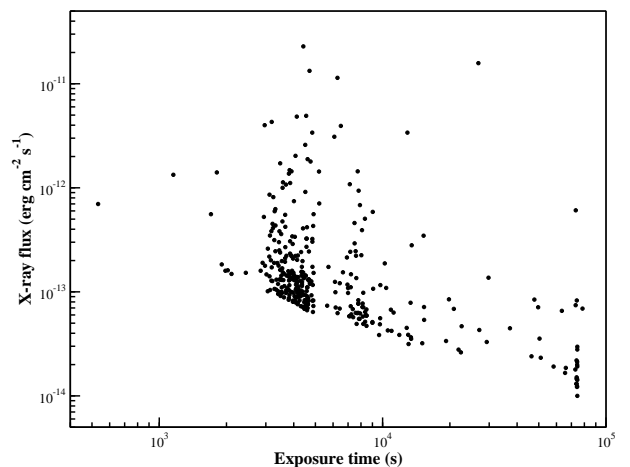


Figure 3. Total exposure for each source of our catalog compared with the respective observed X-ray flux evaluated with PIMMS software for a powerlaw spectra with spectral index 2 and an absorption column density of $5 \times 10^{20} \text{ cm}^{-2}$. We note that this model assumption induce an error of $\sim 8\%$ on the estimated flux.

¹² <http://heasarc.nasa.gov/docs/journal/pimms3.html>

We searched several major radio, IR, optical and UV catalogs for possible counterparts within the positional errors obtained with XRTCENTROID to obtain additional information on the source nature.

For the radio catalogs we considered NVSS (N; Condon et al. 1998), Sydney University Molonglo Sky Survey (SUMSS - S; Bock, Large, & Sadler 1999; Mauch et al. 2003), FIRST (F; Becker, White, & Helfand 1995) and WENSS (W; Rengelink et al. 1997) surveys. For the IR catalogs, we used the WISE (w; Wright et al. 2010) archival observations together with the Two Micron All Sky Survey (2MASS - M; Skrutskie et al. 2006) since each WISE source is already associated with the closest 2MASS object by the default catalog (see Cutri & et al. 2012b, for more details), and the UKIRT Infrared Deep Sky Survey (UKIDSS - UK; Lawrence et al. 2007) archival observations. For the UV catalog, we used the Galaxy Evolution Explorer (GALEX GR6 - g; Martin et al. 2005) archival observations. In addition we searched for optical counterparts, with possible spectra available, in the Sloan Digital Sky Survey (SDSS dr9 - s; e.g. Pâris et al. 2012) and in the Six-degree-Field Galaxy Redshift Survey (6DFGS - 6; Jones et al. 2004, 2009). Finally, we searched for X-ray correspondences in the *Chandra* Source Catalog (CSC - C; e.g. Evans et al. 2010).

As anticipated in Section 3.3, we cross-checked XRT-PC observations with UVOT observations both in UV (u) and optical (o) filters. Then, we also considered the NASA Extragalactic Database (NED)¹³ for other multifrequency information. Finally, we cross correlate our sample with the USNO-B Catalog (U; Monet et al. 2003) to identify the optical counterparts of our γ -ray blazar candidates; this is important to prepare and plan future follow up observations (see Table 3).

In our catalog of 357 X-ray sources we find the following counterparts: 26 in the NVSS catalog, 6 in the SUMSS catalog, 5 in the FIRST catalog, 2 in the WENSS catalog, 41 in the SDSS catalog (2 with spectral observations), 5 in the 6DFGS catalog, 194 in the USNO-B catalog, 44 in the GALEX catalog, 6 in the UKIDSS catalog, 197 in the WISE catalog (94 with 2MASS counterpart) and 1 in the CSC catalog. The results of this association procedure are presented in Table 1 (column 10).

Although a proper counterpart identification would require more sophisticated techniques (see for example Brand et al. 2006), for the scope of this work we are simply presenting a list of counterparts associations only based on positional match. We note that for the 197 X-ray sources for which we find WISE counterparts we only have one multiple match, while for the other catalogs considered here we have 7 multiple matches for SDSS, 1 multiple match for GALEX, and 1 multiple match for UKIDSS. When multiple counterparts were found within the positional error we simply choose the closer one.

We add that we also checked *Planck* PCCS (Planck Collaboration et al. 2013), Catalina CRTS (Drake et al. 2009), ROSAT RASS (Voges et al. 1999), XMM-Newton XMM-MASTER (Arviset et al. 2002) and *Suzaku* SUZAMASTER¹⁴ catalogs, finding no correspondences.

5. CANDIDATE γ -RAY-BLAZAR SELECTION

Recently, D’Abrusco et al. (2013) proposed a classification method to identify γ -ray blazar candidates on the basis

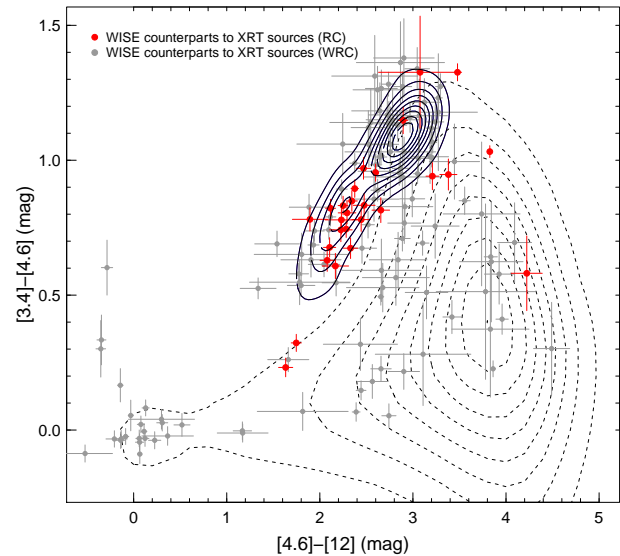


Figure 4. Projection of the three-dimensional WISE color space on the two-dimensional $[3.4]-[4.6]$ $[4.6]-[12]$ color-color plane for XRT-PC sources with a WISE counterpart. Black lines represent the two-dimensional densities of WISE counterparts to known γ -ray blazars evaluated using the KDE technique, with the outermost line indicating the 90% density contour normalized to the peak density. Grey circles represent XRT-PC sources without a radio counterpart (WRC), and red circles represent the XRT-PC sources with a radio counterpart (RC). Black dashed lines represent isodensity contours of generic WISE sources (D’Abrusco et al. 2012; Massaro et al. 2012a). The outer dashed line represent densities $\sim 10^{-4}$ times the peak density.

of their positions in the three-dimensional WISE color space. As a matter of fact, blazars - whose emission is dominated by beamed, non thermal emission - occupy a defined region in such a space, well separated from that occupied by other sources in which thermal emission prevails (D’Abrusco et al. 2012; Massaro et al. 2012a). This method, however can only be applied to WISE sources detected in all 4 WISE bands, i.e., 3.4, 4.6, 12 and 22 μm .

Since 414 out of 610 blazars used by D’Abrusco et al. (2013) are detected in X-rays, we here use the XRT detection as additional information and consider the 148 sources in our catalog with WISE counterparts detected only in the first 3 WISE, bands; we present their projection on the two-dimensional $[3.4]-[4.6]$ $[4.6]-[12]$ color-color plane in Figure 4. In order to select γ -ray blazar-like candidate counterparts among these sources, we evaluate the two-dimensional densities of known γ -ray blazars using the KDE technique (see, e.g., Richards et al. 2004; D’Abrusco, Longo, & Walton 2009; Laurino et al. 2011, and reference therein), and conservatively consider as γ -ray blazar-like candidate counterparts those sources with WISE colors compatible with the 90% KDE density contour normalized to the peak density. On the same figure we indicatively show the isodensity contours of generic WISE sources, clearly showing that γ -ray blazars are well separated on this color-color plane from others sources (see also D’Abrusco et al. 2012; Massaro et al. 2012a).

In this way we select 64 blazar-like candidate counterparts lying in the uncertainty region of 33 UGSs. In particular, among these 33 UGSs the sources 2FGLJ0200.4-4105, 2FGLJ1033.5-5032 2FGLJ1328.5-

¹³ <http://ned.ipac.caltech.edu/>

¹⁴ <http://heasarc.gsfc.nasa.gov/W3Browse/all/suzamaster.html>

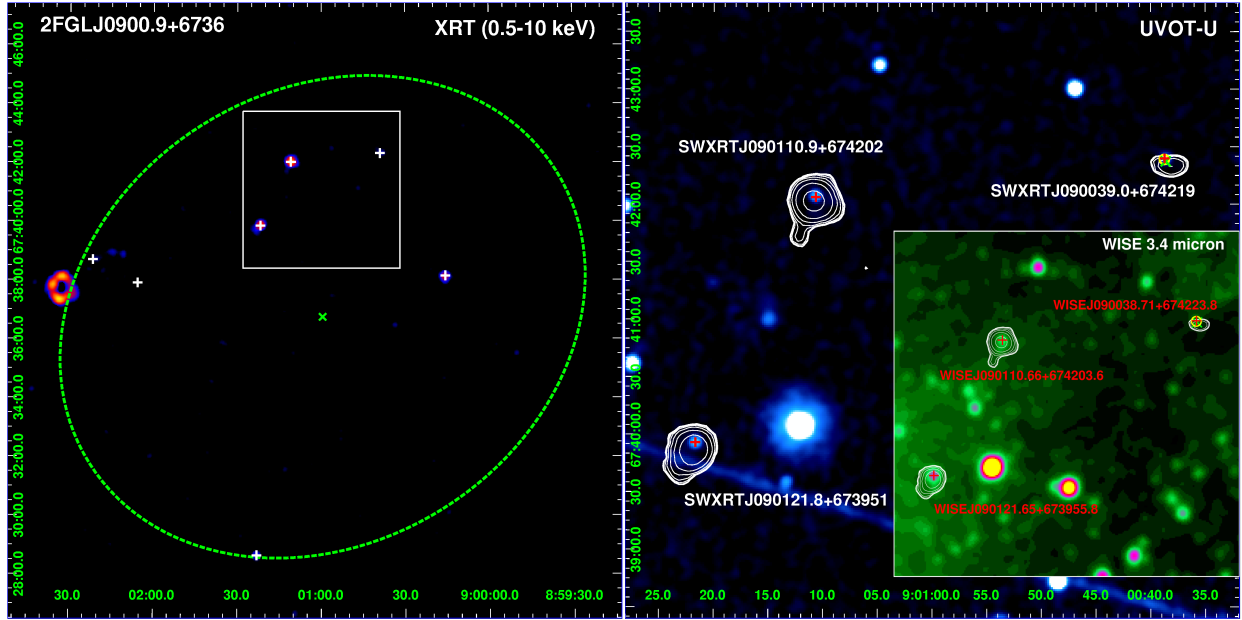


Figure 5. (left frame) Merged XRT-PC image (0.5-10 keV) of the UGS 2FGLJ0900.9+6736. The dashed green ellipse indicates the the positional uncertainty region at 95% level of confidence as reported in 2FGL catalog, and the white crosses indicate the detected X-ray sources. The highly piled-up source on the left is a star clearly visible in UV. (right frame) UVOT-U image of the region indicated in the right frame with the white box, with superimposed X-ray contours in white. Red crosses represent WISE counterparts to X-ray sources, yellow circles represent NVSS counterparts and green x-crosses represent WENSS counterparts. In the inset we show the $3.4\ \mu\text{m}$ WISE image of the same region of right frame, indicating in red the name of the WISE counterparts to X-ray sources.

4728, 2FGLJ1738.9+8716, 2FGLJ2228.6-1633 and 2FGLJ2246.3+1549 feature a unique X-ray counterpart, and are therefore considered γ -ray blazar candidates.

We note that [Massaro et al. \(2013a\)](#) applied the classification method proposed by [D’Abrusco et al. \(2013\)](#) to the same UGSs sample discussed here, selecting 75 blazar-like WISE sources (see Sect. 6.1). Among these 75 sources 28 have an X-ray counterpart in our catalog, and 26 out of these 28 - with the exceptions of SWXRTJ011619.2-615344 and SWXRTJ174507.7+015442 - are also selected as γ -ray blazar-like candidate counterparts with the KDE technique proposed here. This is an excellent agreement, considering that the method proposed by [D’Abrusco et al. \(2013\)](#) makes use of a three-dimensional modelization in the *Principal Component* space, while the KDE contours in Figure 4 represent a two-dimensional source density in the *color* space ([Massaro et al. 2012a](#)). In addition, with the KDE technique we also select the source SWXRTJ060102.8+383829, whose radio counterpart WN0557.5+3838 has been classified as γ -ray blazar-like source by [Massaro et al. \(2013b\)](#) on the basis of its low-frequency radio properties (see Sect. 6.1). We so select 37 new γ -ray blazar-like candidate counterparts, marked in Table 1 (column 10) with the “KDE” string, and present their SEDs in Appendix B.

6. COMPARISON WITH PREVIOUS ANALYSES

6.1. Gamma-ray blazar candidates

As anticipated in Sect. 5, we compare our results with those of [Massaro et al. \(2013a\)](#), that applied the classification method proposed by [D’Abrusco et al. \(2013\)](#) to the same UGSs sample considered in this work, finding 75 blazar-like WISE candidate counterparts in the *Fermi* LAT positional uncertainty region of 61 UGSs. Among these UGSs, for the 35 for which we have available XRT-PC observations

we find no X-ray counterparts only for 5 of them. For the other 30 UGSs, [Massaro et al. \(2013a\)](#) find a total of 44 blazar-like WISE candidate counterparts, and in our catalog we find X-ray counterparts to 28 of the latter. These sources are marked in Table 1 (column 10) with the “WISE” string, and their SEDs are presented in Appendix B. In particular, among these 30 UGSs the sources 2FGLJ0116.6-6153, 2FGLJ0227.7+2249, 2FGLJ0316.1-6434, 2FGLJ0414.9-0855, 2FGLJ0723.9+2901, 2FGLJ1029.5-2022, 2FGLJ1254.2-2203, 2FGLJ1614.8+4703, 2FGLJ1622.8-0314 and 2FGLJ1924.9-1036 feature a unique X-ray counterpart, and are therefore considered γ -ray blazar candidates.

We also compare our results with those of [Massaro et al. \(2013b\)](#), that investigate the low-frequency radio properties of blazars and searched for sources with similar radio properties combining the information derived from the WENSS and NVSS surveys, identifying 26 γ -ray blazar-like sources in the *Fermi* LAT positional uncertainty regions of 21 UGSs. Among these 21 objects, we have available XRT-PC observations for 17 UGSs, and we find no X-ray sources for 3 of them. For the remaining 18 UGSs [Massaro et al. \(2013a\)](#) find a total of 20 γ -ray blazar-like sources, and in our catalog we find an X-ray counterpart to 1 of them - WN0557.5+3838 - namely the source SWXRTJ060102.8+383829 (NVSSJ060102+383828). This source is marked in Table 1 (column 10) with the “WENSS” string, and its SED is presented in Appendix B. We note that SWXRTJ060102.8+383829 is the only X-ray source lying in the uncertainty region of the UGS 2FGLJ0600.9+3839, which we therefore consider a γ -ray blazar candidate.

We stress that these three methods to identify γ -ray blazar-like sources - namely, the one proposed by [D’Abrusco et al. \(2013\)](#) based on three-dimensional WISE colors space, the one proposed by [Massaro et al. \(2013b\)](#) based on low-

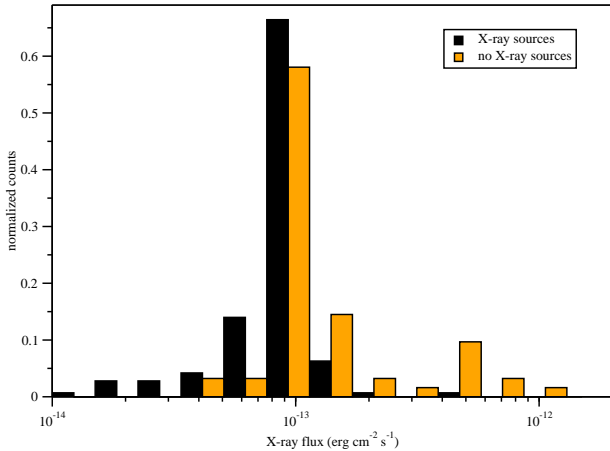


Figure 6. X-ray fluxes reached by XRT-PC observation of the 62 UGSs that show no X-ray counterpart falling in the *Fermi* LAT positional uncertainty region (orange bars) compared with X-ray fluxes reached in the 143 UGSs that show at least one X-ray candidate counterpart (black bars). The flux limit is estimated with the same spectral model considered in Sect. 4 (see Figure 3).

frequency radio properties, and the KDE technique applied to the two-dimensional WISE colors space - do not necessarily select the same sources (see Tables 5 and 6), nor do they necessarily select the brighter X-ray candidate counterpart of the UGS. As an example we show in the left frame of Figure 5 the merged XRT-PC image (0.5-10 keV) of the UGS 2FGLJ0900.9+6736 (the bright, highly piled-up source on the left is a star, clearly visible in UV). The dashed green ellipse indicates the positional uncertainty region at 95% level of confidence as reported in 2FGL catalog. In the right frame of the same Figure we show the UVOT-U merged image of the region indicated in the left frame with the white box, with superimposed X-ray contours. This region contains the γ -ray blazar-like source SWXRTJ090121.8+673951, with a count rate of $5.87 \pm 1.10 \cdot 10^{-3}$ ph s^{-1} , selected on the basis of the IR colors of its WISE counterpart. However, the brighter X-ray source detected in the LAT positional uncertainty region is SWXRTJ090110.9+674202, with a count rate of $7.07 \pm 1.10 \cdot 10^{-3}$ ph s^{-1} is not selected as γ -ray blazar-like source, as well as SWXRTJ090039.0+674219, with a count rate of $1.52 \pm 0.53 \cdot 10^{-3}$ ph s^{-1} , which is the only X-ray source in the LAT positional uncertainty region that shows a radio counterpart within the XRT-PC positional error - namely NVSSJ090038+674223 (indicated with a yellow circle) and WN0856.1+6754 (indicated with a green x-cross). Finally, SWXRTJ090123.0+672838 (the southernmost X-ray source shown in the left frame of 5, is selected as a γ -ray blazar-like source with the KDE technique and has a count rate of $1.33 \pm 0.49 \cdot 10^{-3}$ ph s^{-1} .

6.2. Sources without counterparts

As anticipated in Section 4, 62 UGSs of our sample (most of them lying on the Galactic plane), although featuring XRT-PC observations, show no X-ray counterpart. The X-ray fluxes reached by XRT-PC observations of these sources are presented in Figure 6 in comparison with the X-ray fluxes reached for UGSs that show X-ray candidate counterparts. The flux limit is estimated with the same spectral model considered in Sect. 4 (see Figure 3). We see that the obser-

vations of sources that show at least one X-ray candidate counterpart reach lower fluxes $\sim 10^{-14}$ erg cm^{-2} s^{-1} with respect to observations of sources that show no X-ray counterparts, the latter reaching fluxes $\sim 4 \times 10^{-14}$ erg cm^{-2} s^{-1} . The two observations, however peak at the same X-ray flux of $\sim 10^{-13}$ erg cm^{-2} s^{-1} . In particular we have 45 UGSs that, despite a total exposure time > 3 ks, do not show any X-ray counterpart. Moreover, we note that 7 of these UGSs - namely 2FGLJ0002.7+6220, 2FGLJ0248.5+5131, 2FGLJ0332.1+6309, 2FGLJ0431.5+3622, 2FGLJ0602.7-4011, 2FGLJ1032.9-8401 and 2FGLJ1759.2-3853 - have a γ -ray blazar-like candidate counterpart in their positional uncertainty region, as reported by Massaro et al. (2013a) and Massaro et al. (2013b).

Moreover, we have 35 UGSs that, in their *Fermi* LAT positional uncertainty region, show X-ray candidate counterparts in XRT-PC observations, but without lower energy counterparts in either UVOT observations or the catalogs we described in Section 4. To take into account the astrometric uncertainties of these catalogs, we searched for counterpart of these sources using a searching radius equal to three times the positional error obtained with XRT-CENTROID, yielding 6 UGS - namely 2FGLJ0239.5+1324, 2FGLJ0644.6+6034, 2FGLJ0745.5+7910, 2FGLJ1544.5-1126, 2FGLJ1842.3-5839 and 2FGLJ2133.5-6431 - that show an X-ray candidate counterpart without lower energy counterparts. We present a list of these sources in Table 4, that can be useful for follow up observations aiming at determine their exact nature.

6.3. Comparison with 1FGL catalog

We note that among the 299 UGSs analyzed, there are 66 sources that were also unidentified according to the investigation performed in the first *Fermi* γ -ray catalog (1FGL) but have been classified as active galactic nuclei (AGNs) or as pulsars (PSRs) using two different statistical approaches: the Classification Tree and the Logistic regression analyses (see Ackermann et al. 2012, and references therein). In particular, 38 out of the 66 show γ -ray properties similar to those of others γ -ray AGNs while 11 are potential PSRs with the remaining 17 of unknown origin.

For the 49 UGSs classified on the basis of the above statistical methods, we performed a comparison with our results in particular to check if the 2FGL sources having in their uncertainty region an X-ray source whose IR counterpart features blazar-like WISE colors according to the KDE technique illustrated in Sect. 5 were also classified as AGNs according to the results of Ackermann et al. (2012). We found that 8 out of 33 UGSs we associate with a γ -ray blazar-like source are also classified as AGNs, all of them with a probability systematically higher than 60%. There is only one case (i.e., 2FGL 1328.5-4728) in which the statistical procedures assigned a PSR classification, with a low probability (i.e., 53%) while the KDE method identified the X-ray candidate counterpart of the *Fermi* source as a blazar-like object.

7. SUMMARY AND CONCLUSIONS

In this work we present a catalog of X-ray sources lying in the positional uncertainty regions of the 299 UGSs reported in the 2FGL catalog without any γ -ray analysis flag. To this end, we made use of all available observations performed by *Swift* XRT in PC mode up to March 31, 2013, that were available for 205 UGSs. In order to detect the fainter sources, we

merged all the observations corresponding to each UGSs, and applied to these merged observations different detection algorithms (i.e., `XIMAGE DETECT` and `SOSTA`). The source list was cleaned from spurious and extended sources by visual inspection of all the observations, to yield a final catalog of 357 X-ray sources. We searched several major radio, IR, optical and UV surveys for any possible counterparts within the positional error of our X-ray sources to obtain additional information on their nature, providing a comprehensive list of X-ray sources with multi-wavelength properties.

The main results of our analysis can be summarized as follows:

- We find X-ray candidate counterparts for $\sim 70\%$ of the UGSs investigated. In particular, we have $\sim 25\%$ UGSs featuring a single X-ray counterpart and $\sim 45\%$ UGSs featuring multiple X-ray candidate counterparts falling in the positional uncertainty region at 95% level of confidence.
- For each X-ray source we also looked in the corresponding UVOT merged images for UV-optical counterparts performing sources photometry, and finding UV-optical counterparts to $\sim 71\%$ of the X-ray sources in our catalog.
- We find no X-ray counterparts for 62 UGSs in our sample ($\sim 30\%$), 46 of which have a total exposure ≥ 3 ks.
- Comparing our results with [Massaro et al. \(2013a\)](#) and [Massaro et al. \(2013b\)](#) we find X-ray candidate counterparts to 29 sources classified as γ -ray blazar-like.
- Applying the KDE technique to IR colors of WISE counterparts, we obtain an additional list of 37 γ -ray blazar-like sources for 33 UGSs (29 with a unique candidate and 4 with a double candidate). In particular, 10 out of these 33 2FGL sources have radio counterparts, and for 4 UGSs out of 33 we add a different γ -ray blazar-like sources from those selected by [Massaro et al. \(2013a\)](#) and [Massaro et al. \(2013b\)](#).
- Among the 51 UGSs that have a single X-ray counterpart, 17 have their X-ray counterpart selected as γ -ray blazar-like source with the three methods discussed above, and are there considered as γ -ray blazar candidates.
- The source 2FGL1328.5-4728, a γ -ray blazar candidate selected with the KDE technique, is classified as PSR by [Ackermann et al. \(2012\)](#).

Even though blazars are expected to be bright in X-rays, the methods discussed here to find γ -ray blazar-like sources in UGSs uncertainty regions show that this is not always the case.

We note that 39 2FGL sources in our sample are in common with the analysis of 1FLG UGSs by [Takeuchi et al. 2013](#)). Comparing our results with [Ackermann et al. \(2012\)](#) we note that 38 2FGL sources in our sample are classified as AGN the 1FGL catalog with high level of confidence, 11 2FGL sources in our sample are classified as PSR with low level of confidence, and 17 2FGL sources in our sample are unclassified. In particular, 8 2FGL sources with a γ -ray blazar-like source selected with the KDE technique are classified as AGN by [Ackermann et al. \(2012\)](#).

Ground-based, optical and near IR, spectroscopic follow up observations will be planned for the *Swift* XRT sources selected as γ -ray blazar-like candidate counterparts because they are crucial to confirm the nature of the selected sources and to obtain their redshift, as shown for the unidentified INTEGRAL and *Swift* sources (e.g., [Masetti et al. 2012](#); [Parisi et al. 2012](#), and references therein).

We acknowledge useful comments and suggestions by our anonymous referee. The authors gratefully acknowledge A. Falcone for the *Swift* XRT Survey of *Fermi* Unassociated Sources that produced most of the observations used in this work. F. Massaro is grateful to M. Ajello for his support. The work is supported by the NASA grants NNX12AO97G. R. D'Abrusco gratefully acknowledges the financial support of the US Virtual Astronomical Observatory, which is sponsored by the National Science Foundation and the National Aeronautics and Space Administration. H. A. Smith acknowledges partial support from NASA/JPL grant RSA 1369566. The work by G. Tosti is supported by the ASI/INAF contract I/005/12/0. TOPCAT¹⁵ ([Taylor 2005](#)) for the preparation and manipulation of the tabular data and the images. The WENSS project was a collaboration between the Netherlands Foundation for Research in Astronomy and the Leiden Observatory. We acknowledge the WENSS team consisted of Ger de Bruyn, Yuan Tang, Roeland Rengelink, George Miley, Huub Rottgering, Malcolm Bremer, Martin Bremer, Wim Brouw, Ernst Raimond and David Fullagar for the extensive work aimed at producing the WENSS catalog. Part of this work is based on archival data, software or on-line services provided by the ASI Science Data Center. This research has made use of data obtained from the High Energy Astrophysics Science Archive Research Center (HEASARC) provided by NASA's Goddard Space Flight Center; the SIMBAD database operated at CDS, Strasbourg, France; the NASA/IPAC Extragalactic Database (NED) operated by the Jet Propulsion Laboratory, California Institute of Technology, under contract with the National Aeronautics and Space Administration. This research has made use of software provided by the Chandra X-ray Center (CXC) in the application packages CIAO, ChIPS, and Sherpa. Part of this work is based on the NVSS (NRAO VLA Sky Survey); The National Radio Astronomy Observatory is operated by Associated Universities, Inc., under contract with the National Science Foundation. This publication makes use of data products from the Two Micron All Sky Survey, which is a joint project of the University of Massachusetts and the Infrared Processing and Analysis Center/California Institute of Technology, funded by the National Aeronautics and Space Administration and the National Science Foundation. This publication makes use of data products from the Wide-field Infrared Survey Explorer, which is a joint project of the University of California, Los Angeles, and the Jet Propulsion Laboratory/California Institute of Technology, funded by the National Aeronautics and Space Administration. Funding for the SDSS and SDSS-II has been provided by the Alfred P. Sloan Foundation, the Participating Institutions, the National Science Foundation, the U.S. Department of Energy, the National Aeronautics and Space Administration, the Japanese Monbukagakusho, the Max Planck Society, and the

¹⁵ <http://www.star.bris.ac.uk/mbt/topcat/>

Higher Education Funding Council for England. The SDSS Web Site is <http://www.sdss.org/>. The SDSS is managed by the Astrophysical Research Consortium for the Participating Institutions. The Participating Institutions are the American Museum of Natural History, Astrophysical Institute Potsdam, University of Basel, University of Cambridge, Case Western Reserve University, University of Chicago, Drexel University, Fermilab, the Institute for Advanced Study, the Japan Participation Group, Johns Hopkins University, the Joint Institute for Nuclear Astrophysics, the Kavli Institute for Particle Astrophysics and Cosmology, the Korean Scientist Group, the Chinese Academy of Sciences (LAMOST), Los Alamos National Laboratory, the Max-Planck-Institute for Astronomy (MPIA), the Max-Planck-Institute for Astrophysics (MPA), New Mexico State University, Ohio State University, University of Pittsburgh, University of Portsmouth, Princeton University, the United States Naval Observatory, and the University of Washington. The United Kingdom Infrared Telescope is operated by the Joint Astronomy Centre on behalf of the Science and Technology Facilities Council of the U.K. The CSS survey is funded by the National Aeronautics and Space Administration under Grant No. NNG05GF22G issued through the Science Mission Directorate Near-Earth Objects Observations Program. The CRTS survey is supported by the U.S. National Science Foundation under grants AST-0909182.

REFERENCES

- Abdo A. A., et al., 2009, *Aph*, 32, 193
 Abdo A. A., et al., 2010a, *ApJ*, 712, 1209
 Abdo A. A., et al., 2010b, *ApJ*, 712, 957
 Abdo A. A., et al., 2010c, *ApJS*, 188, 405
 Ackermann M., et al., 2011, *ApJ*, 743, 171
 Ackermann M., et al., 2012, *ApJ*, 753, 83
 Ackermann M., et al., 2012, *ApJ*, 753, 83
 Ackermann M., et al., 2013, *Sci*, 339, 807
 Arnaud K. A., 1996, *ASPC*, 101, 17
 Aleksić J., et al., 2012, *A&A*, 544, A142
 Aliu E., et al., 2011, *ApJ*, 742, 127
 Arviset C., Guainazzi M., Hernandez J., Dowson J., Osuna P., Venet A., 2002, *astro*, arXiv:astro-ph/0206412
 Atwood W. B., et al., 2009, *ApJ*, 697, 1071
 Becker R. H., White R. L., Helfand D. J., 1995, *ApJ*, 450, 559
 Blandford R. D., Rees M. J., 1978, *Proc. "Pittsburgh Conference on BL Lac objects"*, 328
 Bock D. C.-J., Large M. I., Sadler E. M., 1999, *AJ*, 117, 1578
 Brand, K., Brown, M. J. I., Dey, A., et al. 2006, *ApJ*, 641, 140
 Burrows D. N., et al., 2005, *SSRv*, 120, 165
 Capalbi M., Perri M., Saija B., Tamburelli F., Angelini L. 2005, http://heasarc.nasa.gov/docs/swift/analysis/xrt_swgguide_v1_2.pdf
 Cardelli J. A., Clayton G. C., Mathis J. S., 1989, *ApJ*, 345, 245
 Casandjian J.-M., Grenier I. A., 2008, *A&A*, 489, 849
 Casanova S., et al., 2010, *PASJ*, 62, 769
 Cheung C. C., Donato D., Gehrels N., Sokolovsky K. V., Giroletti M., 2012, *ApJ*, 756, 33
 Condon J. J., Cotton W. D., Greisen E. W., Yin Q. F., Perley R. A., Taylor G. B., Broderick J. J., 1998, *AJ*, 115, 1693
 Cutri R. M., et al., 2012a, *wise.rept*, 1
 Cutri R. M., et al., 2012b, *yCat*, 2311, 0
 Dai X., Bregman J. N., Kochanek C. S., 2012, *AAS*, 219, #415.06
 D'Abrusco R., Longo G., Walton N. A., 2009, *MNRAS*, 396, 223
 D'Abrusco R., Massaro F., Ajello M., Grindlay J. E., Smith H. A., Tosti G., 2012, *ApJ*, 748, 68
 D'Abrusco R., Massaro F., Paggi A., Masetti N., Tosti G., Giroletti M., Smith H. A., 2013, *ApJS*, 206, 12
 D'Elia V., et al., 2013, *A&A*, 551, A142
 Dermer C. D., Schlickeiser R., 1993, *ApJ*, 416, 458
 Dermer C. D., Schlickeiser R., 2002, *ApJ*, 575, 667
 Dermer C. D., Finke J. D., Krug H., Böttcher M., 2009, *ApJ*, 692, 32
 Dermer C. D., Powale G., 2013, *A&A*, 553, A34
 Drake, A. J., Djorgovski, S. G., Mahabal, A., et al. 2009, *ApJ*, 696, 870
 Eckart M. E., McGreer I. D., Stern D., Harrison F. A., Helfand D. J., 2010, *ApJ*, 708, 584
 Elvis M., Plummer D., Schachter J., Fabbiano G., 1992, *ApJS*, 80, 257
 Evans I. N., et al., 2010, *ApJS*, 189, 37
 Finke J. D., Dermer C. D., Böttcher M., 2008, *ApJ*, 686, 181
 Finke J. D., 2013, *ApJ*, 763, 134
 Freeman P., Doe S., Siemiginowska A., 2001, *SPIE*, 4477, 76
 Fruscione A., et al., 2006, *SPIE*, 6270,
 Fujinaga T., et al., 2011, *PASJ*, 63, 857
 Gehrels N., Michelson P., 1999, *Aph*, 11, 277
 Ghirlanda G., Ghisellini G., Tavecchio F., Foschini L., 2010, *MNRAS*, 407, 791
 Giommi P., Padovani P., 1994, *MNRAS*, 268, L51
 Giommi P., et al., 2012, *A&A*, 541, A160
 Hartman R. C., et al., 1999, *ApJS*, 123, 79
 H.E.S.S. Collaboration, et al., 2013, *A&A*, 552, A118
 Inoue S., Takahara F., 1996, *ApJ*, 463, 555
 Kalberla P. M. W., Burton W. B., Hartmann D., Arnal E. M., Bajaja E., Morras R., Pöppel W. G. L., 2005, *A&A*, 440, 775
 Kataoka J., et al., 2012, *ApJ*, 757, 176
 Kovalev Y. Y., 2009a, *ApJ*, 707, L56
 Kovalev Y. Y., et al., 2009b, *ApJ*, 696, L17
 Jones D. H., et al., 2004, *MNRAS*, 355, 747
 Jones D. H., et al., 2009, *MNRAS*, 399, 683
 Landt H., Padovani P., Perlman E. S., Giommi P., Bignall H., Tzioumis A., 2001, *MNRAS*, 323, 757
 Laurino O., D'Abrusco R., Longo G., Riccio G., 2011, *MNRAS*, 418, 2165
 Lawrence A., et al., 2007, *MNRAS*, 379, 1599
 Yan H., Lazarian A., Schlickeiser R., 2012, *ApJ*, 745, 140
 Maeda K., et al., 2011, *ApJ*, 729, 103
 Mahony E. K., Sadler E. M., Murphy T., Ekers R. D., Edwards P. G., Massardi M., 2010, *ApJ*, 718, 587
 Maselli A., Massaro E., Nesci R., Sclavi S., Rossi C., Giommi P., 2010, *A&A*, 512, A74
 Maselli A., et al., 2013, *ApJS*, 206, 17
 Masetti N., et al., 2012, *A&A*, 538, A123
 Massaro F., Giommi P., Tosti G., Cassetti A., Nesci R., Perri M., Burrows D., Gehrels N., 2008a, *A&A*, 489, 1047
 Massaro F., Tramacere A., Cavaliere A., Perri M., Giommi P., 2008b, *A&A*, 478, 395
 Massaro F., Tramacere A., Cavaliere A., Perri M., Giommi P., 2011a, *A&A*, 528, 1
 Massaro F., Paggi A., Elvis M., Cavaliere A., 2011b, *ApJ*, 739, 73
 Massaro F., Paggi A., Cavaliere A., 2011c, *ApJ*, 742, L32
 Massaro F., D'Abrusco R., Tosti G., Ajello M., Gasparrini D., Grindlay J. E., Smith H. A., 2012a, *ApJ*, 750, 138
 Massaro F., D'Abrusco R., Paggi A., Masetti N., Giroletti M., Tosti G., Smith H. A., Funk S., 2013, *ApJS*, 206, 13
 Massaro F., D'Abrusco R., Paggi A., Masetti N., Giroletti M., Tosti G., Smith H. A., Funk S., 2013, *ApJS*, in press
 Martin D. C., et al., 2005, *ApJ*, 619, L1
 Mauch T., Murphy T., Buttery H. J., Curran J., Hunstead R. W., Piestrzynski B., Robertson J. G., Sadler E. M., 2003, *MNRAS*, 342, 1117
 Mirabal N., Halpern J. P., Eracleous M., Becker R. H., 2000, *ApJ*, 541, 180
 Mirabal N., 2009, arXiv, arXiv:0908.1389
 Mirabal N., Halpern J. P., 2009, *ApJ*, 701, L129
 Mirabal N., Nieto D., Pardo S., 2010, arXiv, arXiv:1007.2644
 Monet D. G., et al., 2003, *AJ*, 125, 984
 Moretti A., et al., 2005, *SPIE*, 5898, 360
 Moretti A., et al., 2007, *SPIE*, 6688,
 Moretti A., Vattakunnel S., Tozzi P., Salvaterra R., Severgnini P., Fugazza D., Haardt F., Gilli R., 2012, *A&A*, 548, A87
 Mori H., Maeda Y., Ueda Y., Dotani T., Ishida M., 2012, *PASJ*, 64, 112
 Mukherjee R., et al., 1997, *ApJ*, 490, 116
 Murakami H., Kitamoto S., Kawachi A., Nakamori T., 2011, *PASJ*, 63, 873
 Nolan P. L., et al., 2012, *ApJS*, 199, 31
 Oezel M. E., Thompson D. J., 1996, *ApJ*, 463, 105
 Padovani P., Giommi P., 1995, *ApJ*, 444, 567
 Pâris I., et al., 2012, *A&A*, 548, A66
 Parisi P., et al., 2012, *A&A*, 545, A101
 Planck Collaboration, et al., 2013, arXiv, arXiv:1303.5088
 Park S. Q., et al., 2010, *ApJ*, 717, 1181
 Perlman E. S., Padovani P., Giommi P., Sambruna R., Jones L. R., Tzioumis A., Reynolds J., 1998, *AJ*, 115, 1253
 Perlman E. S., Schachter J. F., Stocke J. T., 1999, *AAS*, 31, 1396
 Perlman E. S., 2000, *AIPC*, 515, 53

- Perri M., et al., 2007, A&A, 462, 889
Petrov L., Mahony E. K., Edwards P. G., Sadler E. M., Schinzel F. K.,
McConnell D., 2013, MNRAS, 432, 1294
Puccetti S., et al., 2011, A&A, 528, A122
Rau A., et al., 2012, A&A, 538, A26
Reimer O., 2001, ASSL, 267, 17
Rengelink R. B., Tang Y., de Bruyn A. G., Miley G. K., Bremer M. N.,
Roettgering H. J. A., Bremer M. A. R., 1997, A&AS, 124, 259
Richards G. T., et al., 2004, ApJS, 155, 257
Roming P. W. A., et al., 2005, SSRv, 120, 95
Skrutskie M. F., et al., 2006, AJ, 131, 1163
Sowards-Emmerd D., Romani R. W., Michelson P. F., 2003, ApJ, 590, 109
Stern D., et al., 2005, ApJ, 631, 163
Stern D., et al., 2012, ApJ, 753, 30
Su M., Finkbeiner D. P., 2012, arXiv, arXiv:1207.7060
Takeuchi, Y., Kataoka, J., Maeda, K., et al. 2013, arXiv:1307.5581
Taylor M. B., 2005, ASPC, 347, 29
Thompson D. J., 2008, RPPh, 71, 116901
Tramacere A., et al., 2007, A&A, 467, 501
Vandenbroucke J., et al., 2010, ApJ, 718, L166
Voges W., et al., 1999, A&A, 349, 389
White R. L., Becker R. H., Helfand D. J., Gregg M. D., 1997, ApJ, 475, 479
Wright E. L., et al., 2010, AJ, 140, 1868
Zechlin H.-S., Fernandes M. V., Elsässer D., Horns D., 2012, A&A, 538,
A93

APPENDIX

A. CATALOG TABLES

Here we present the catalog of X-ray sources with their main properties.

In Table 1 we list all the X-ray sources found in XRT-PC observations in the positional uncertainty region of each UGS. The columns contain the following information: (1) NAME XRT: source designation as described in Section 3 and corresponding 2FGL UGS; (2) OTHER NAME: name of the counterpart found in the catalogs described in Section 4. If more than one counterpart is found, the order we choose for the alternate name is the following: NVSS, FIRST, SUMSS, WENSS, WISE, SDSS, 6DFGS, NED; (3) RA: right ascension as given by XRTCENTROID; (4) DEC: declination as given by XRTCENTROID; (5) ERR: positional error in arcseconds as given by XRTCENTROID; (6) EXP: XRT-PC total exposure in seconds; (7) COUNTRATE: countrate and relative error as given by DETECT in 10^{-3}ph s^{-1} ; (8) SIGN: signal to noise threshold above which the source is detected by DETECT; (9) SOSTA: countrate and relative error as given by SOSTA in 10^{-3}ph s^{-1} ; (10) SNR: signal to noise ratio as given by SOSTA; (11) NOTES: results of the cross-matching with the catalogs discussed in Section 4 within the positional error reported in column ERR: NVSS=N, FIRST=F, SUMSS=S, WENSS=W, WISE=w, 2MASS=M, UKIDSS=UK, SDSS=s, 6=6DFGS, GALEX=g, UVOT(optical filter)=o, UVOT(UV filter)=u, USNO-B=U, CSC=C; (12) CAND: γ -ray blazar-like sources according to Massaro et al. (2013a) (WISE), to Massaro et al. (2013b) (WENSS) and to the KDE technique as discussed in Section 6.1; (12) REDSHIFT: redshift for the source counterpart as reported by SDSS, 6DFGS or NED.

In Table 2 we list, for each source in Table 1, the properties of the UV-optical counterpart found in merged UVOT observations. The columns contain the following information: (1) NAME XRT: source designation as described in Section 3 and corresponding 2FGL UGS; (2) RA: right ascension of the UVOT counterpart; (3) DEC: declination UVOT counterpart; (4) SEP: angular separation in arcseconds between the XRT-PC source and the UVOT counterpart; (5) E(B-V): galactic extinction value as derived by the Infrared Science Archive¹⁶ (IRSA); (6) EXPV: exposure of the UVOT-V filter merged observation in seconds; (7) MAGV: UVOT-V filter magnitude (Vega system) and relative error as given by UVOTSOURCE (not corrected by galactic extinction). Upper limits are indicated with 0.00 errors, while * indicate filter saturation; (8) MAGVS: UVOT-V filter magnitude (Vega system) and relative error as given by UVOTDETECT (not corrected by galactic extinction). Upper limits are indicated with 0.00 errors, while * indicate filter saturation; (9) EXPB, (10) MAGB, (11) MAGBS: same as columns (6), (7) and (8) but for UVOT-B filter; (12) EXPU, (13) MAGU, (14) MAGUS: same as columns (6), (7) and (8) but for UVOT-U filter; (15) EXPW1, (16) MAGW1, (17) MAGW1S: same as columns (6), (7) and (8) but for UVOT-W1 filter; (18) EXPM2, (19) MAGM2, (20) MAGM2S: same as columns (6), (7) and (8) but for UVOT-M2 filter; (21) EXPW2, (22) MAGW2, (23) MAGW2S: same as columns (6), (7) and (8) but for UVOT-W2 filter.

In Table 3 we list all the XRT-PC sources that features a USNO-B counterpart within the positional error and present the magnitudes of this counterpart. The columns contain the following information: (1) NAME XRT: source designation as described in Section 3; (2) B1: first epoch blue magnitude; (3) B2: second epoch blue magnitude; (4) R1: first epoch red magnitude; (5) R2: second epoch red magnitude; (6) I: second epoch near-IR magnitude.

In Table 4 we list all UGS that, although featuring XRT-PC observations, show no X-ray counterpart. The columns contain the following information: (1) NAME 2FGL: UGS name as reported in the 2FGL, with boldface indicating those sources that have a γ -ray blazar-like candidate counterpart in their positional uncertainty region as reported by Massaro et al. (2013a) and Massaro et al. (2013b); (2) EXP: XRT-PC total exposure in seconds.

¹⁶ <http://irsa.ipac.caltech.edu/applications/DUST/>

Table 1
Sample catalog of XRT-PC detected sources in the positional uncertainty region of each UGS as reported in the 2FGL. Column description is given in Appendix A.

NAME XRT	OTHER NAME	RA J2000	DEC J2000	ERR arcsec	EXP s	COUNTRATE 10^{-3} ph s $^{-1}$	SIGN	SOSTA 10^{-3} ph s $^{-1}$	SNR	NOTES	CAND	REDSHIFT
2FGLJ0031.0+0724												
SWXRTJ003054.8+072324	WISEJ003054.91+072323.7	00:30:54.817	+07:23:24.33	5.70	8137	1.87(0.60)	3	1.55(0.59)	2.61	w.M,UK,s,g.o.u.U		
SWXRTJ003113.1+073143	SDSSJ003112.79+073143.6	00:31:13.114	+07:31:43.31	4.78	7571	5.95(1.00)	5	6.42(1.10)	6.07	UK,s.o.u		
SWXRTJ003119.9+072452	FIRSTJ003119.7+072454	00:31:19.927	+07:24:52.48	4.06	7914	16.50(1.60)	5	16.19(1.60)	9.92	F.w,UK,s.o.u.U	KDE	
2FGLJ0039.1+4331												
SWXRTJ003858.3+432947	WISEJ003858.27+432947.0	00:38:58.261	+43:29:46.82	5.11	3956	6.98(1.60)	4	7.60(1.60)	4.61	w.M,o.U		WISE
SWXRTJ003908.5+433027		00:39:08.475	+43:30:27.46	5.76	4093	2.84(1.10)	2	2.84(1.10)	2.57			
SWXRTJ003938.4+433446		00:39:38.387	+43:34:46.23	5.35	4265	2.35(0.94)	2	2.58(1.00)	2.55			

Table 3

Sample of XRT-PC sources featuring a USNO-B counterpart within the positional error. Column description is given in Appendix A.

NAME XRT	B1	B2	R1	R2	I
SWXRTJ003054.8+072324	19.85	18.32	19.48	18.24	18.28
SWXRTJ003119.9+072452	19.03	18.17	19.84	18.63	18.67

B. BLAZAR-LIKE SOURCES SPECTRAL ENERGY DISTRIBUTIONS

Here we present the XRT-PC counterparts of γ -ray blazar-like sources, with their SEDs.

In Table 5 we list the 30 XRT-PC counterparts of γ -ray blazar-like sources according to the classification methods proposed by D’Abrusco et al. (2013) and Massaro et al. (2013b). In boldface we indicate sources with radio counterparts within the positional error listed in Table 1. Columns contain the following information: (1) NAME 2FGL: UGS name as reported in the 2FGL; (2) NAME XRT: source designation as described in Section 3; (3) ALT NAME: name of the WISE counterpart (as reported by WISE All-Sky data catalog, Cutri & et al. 2012b) or of the WENSS counterpart (as reported by WENSS catalog, Rengelink et al. 1997) closer to the XRT-PC coordinates (as reported in Table 1); (4) CLASS: for γ -ray blazar-like sources selected by D’Abrusco et al. (2013), every source is assigned to class A, B, or C depending on the probability of the WISE source to be compatible with the model of the WISE *Fermi* Blazar (WFB) locus: class A sources are considered the most probable candidate blazars for the high-energy source, while class B and class C sources are less compatible with the WFB locus but are still deemed as candidate blazars. For γ -ray blazar-like sources selected by Massaro et al. (2013b), with A we indicate radio sources having $-1.00 \leq \alpha_{325}^{1400} \leq 0.55$ and with B those with $0.55 \leq \alpha_{325}^{1400} \leq 0.65$, where α_{325}^{1400} is the radio spectral index between 325 MHz and 1.4 GHz; (4) TYPE: classification of the candidate blazar according to D’Abrusco et al. (2013) based on the compatibility of the WISE source with the regions of the WFB locus model. BZB and BZQ indicate the regions dominated by BL Lac objects and FSRQs sources respectively, while MIXED indicate the region where the population is mixed in terms of spectral classes.

In Table 6 we list the 44 XRT-PC counterparts of γ -ray blazar-like sources according to the KDE technique illustrated in Sect. 5. In boldface we indicate sources with radio counterparts within the positional error listed in Table 1. Columns contain the following information: (1) NAME 2FGL: UGS name as reported in the 2FGL; (2) NAME XRT: source designation as described in Section 3; (3) WISE NAME: name of the WISE counterpart (as reported by WISE All-Sky data catalog).

SEDs of the sources listed in Table 5 are presented in Figures 7 and 8 for sources that feature and do not feature a radio counterpart within the XRT positional error, respectively. In the same way, SEDs of the sources listed in Table 6 are presented in Figures 9 and 10 for sources that feature and do not feature a radio counterpart within the XRT positional error, respectively. For each XRT-PC source we show the spectral points corresponding to the various counterparts we found in the XRT-PC positional error as reported in Table 1 (see Section 4). Circles represent detections, while down triangles represent upper limits, with the color code presented in the legends. For IR, optical and UV points we present both observed (empty symbols) and de-reddened (full symbols) fluxes, the latter obtained using the extinction law presented by Cardelli, Clayton, & Mathis (1989) and the galactic extinction value as derived by IRSA. When possible, XRT-PC spectra are obtained from events extracted with XRTPRODUCTS task using a 20 pixel radius circle centered on the coordinates reported in Table 1 and background estimated from a nearby source-free circular region of 20 pixel radius. When the source count rate is above $0.5 \text{ counts s}^{-1}$, the data are significantly affected by pileup in the inner part of the point-spread function (Moretti et al. 2005). To remove the pile-up contamination, we extract only events contained in an annular region centered on the source (e.g., Perri et al. 2007). The inner radius of the region was determined by comparing the observed profiles with the analytical model derived by Moretti et al. (2005) and typically has a 4 or 5 pixels radius, while the outer radius is 20 pixels for each observation. Source spectra are binned to ensure a minimum of 20 counts per bin in order to ensure the validity of χ^2 statistics. We performed our spectral analysis with the SHERPA¹⁷ modeling and fitting application (Freeman, Doe, & Siemiginowska 2001) include in the CIAO (Fruscione et al. 2006) 4.5 software package, and with the XSPEC software package, version 12.8.0 (Arnaud 1996) with identical results. For the spectral fitting we used a model comprising an absorption component fixed to the Galactic value (Kalberla et al. 2005) and a powerlaw, and we plot intrinsic fluxes (i.e., without Galactic photoelectric absorption). When the extracted counts are not enough to provide acceptable spectral fits we simply converted the count rates reported in Table 1 to 0.3-10 keV intrinsic fluxes with PIMMS 4.6b software, assuming a powerlaw spectra with spectral index 2 and an absorption component fixed to the Galactic value. In this case we report with a filled circle the flux corresponding to the countrate as obtained with DETECT and with an empty box the countrate as obtained with SOSTA.

¹⁷ <http://cxc.harvard.edu/sherpa>

Table 4

UGSs without XRT-PC counterparts in the *Fermi* LAT positional uncertainty region. In boldface we indicate those sources that have a γ -ray blazar-like candidate counterpart in their uncertainty region as reported by [Massaro et al. \(2013a\)](#) and [Massaro et al. \(2013b\)](#).

NAME 2FGL	EXP s
2FGLJ0002.7+6220	4817
2FGLJ0032.7-5521	3966
2FGLJ0106.5+4854	2889
2FGLJ0237.9+5238	4445
2FGLJ0248.5+5131	2407
2FGLJ0312.8+2013	4099
2FGLJ0332.1+6309	5150
2FGLJ0340.5+5307	4977
2FGLJ0359.5+5410	4320
2FGLJ0418.9+6636	5319
2FGLJ0426.7+5434	4380
2FGLJ0431.5+3622	4433
2FGLJ0516.7+2634	4632
2FGLJ0524.1+2843	3699
2FGLJ0545.6+6018	3988
2FGLJ0600.8-1949	979
2FGLJ0602.7-4011	1930
2FGLJ0854.7-4501	4997
2FGLJ0953.6-1504	3504
2FGLJ1032.9-8401	7999
2FGLJ1208.5-6240	3738
2FGLJ1306.2-6044	4867
2FGLJ1400.2-2412	659
2FGLJ1400.7-1438	417
2FGLJ1410.4+7411	3611
2FGLJ1422.3-6841	3421
2FGLJ1458.5-2121	3374
2FGLJ1513.9-2256	3316
2FGLJ1521.8-5735	5434
2FGLJ1601.1-4220	3394
2FGLJ1617.5-2657	142
2FGLJ1620.8-4928	577
2FGLJ1624.1-4040	3399
2FGLJ1646.7-1333	1508
2FGLJ1702.5-5654	3197
2FGLJ1712.4-3941	604
2FGLJ1744.1-7620	4682
2FGLJ1747.6+0324	3778
2FGLJ1748.9-3923	574
2FGLJ1757.5-6028	4011
2FGLJ1759.2-3853	192
2FGLJ1808.3-3356	727
2FGLJ1816.5+4511	4795
2FGLJ1821.8+0830	380
2FGLJ1849.3-0055	487
2FGLJ1901.1+0427	2957
2FGLJ1902.7-7053	3256
2FGLJ1906.5+0720	10728
2FGLJ1917.0-3027	3666
2FGLJ1949.4-1457	4031
2FGLJ2017.5-1618	3656
2FGLJ2018.0+3626	4368
2FGLJ2028.3+3332	10386
2FGLJ2041.2+4735	3629
2FGLJ2044.4-4757	3771
2FGLJ2107.8+3652	4865
2FGLJ2111.3+4605	5909
2FGLJ2112.5-3042	2844
2FGLJ2117.5+3730	3521
2FGLJ2139.8+4714	3189
2FGLJ2213.7-4754	3326
2FGLJ2347.2+0707	3047

Table 5

XRT-PC counterparts to γ -ray blazar-like sources selected according to D'Abrusco et al. (2013) and Massaro et al. (2013b). In boldface we indicate sources with radio counterparts within the positional error listed in Table 1. Column description is given in Appendix B.

NAME 2FGL	NAME XRT	ALT NAME	CLASS	TYPE
2FGLJ0039.1+4331	SWXRTJ003858.3+432947	WISEJ003858.27+432947.0	C	BZB
2FGLJ0116.6-6153	SWXRTJ011619.2-615344	WISEJ011619.59-615343.5	C	BZB
2FGLJ0133.4-4408	SWXRTJ013306.3-441423	WISEJ013306.35-441421.3	C	BZB
	SWXRTJ013321.5-441319	WISEJ013321.36-441319.4	C	BZQ
2FGLJ0143.6-5844	SWXRTJ014347.1-584551	WISEJ014347.39-584551.3	C	BZB
2FGLJ0227.7+2249	SWXRTJ022744.0+224838	WISEJ022744.35+224834.3	B	BZB
2FGLJ0316.1-6434	SWXRTJ031613.9-643730	WISEJ031614.31-643731.4	C	BZB
2FGLJ0409.8-0357	SWXRTJ040946.5-040002	WISEJ040946.57-040003.4	B	BZB
2FGLJ0414.9-0855	SWXRTJ041457.1-085654	WISEJ041457.01-085652.0	C	MIXED
2FGLJ0600.9+3839	SWXRTJ060102.8+383829	WN0557.5+3838	B	
2FGLJ0644.6+6034	SWXRTJ064459.9+603132	WISEJ064459.38+603131.7	C	MIXED
2FGLJ0723.9+2901	SWXRTJ072355.1+285926	WISEJ072354.83+285929.9	C	BZQ
2FGLJ0746.0-0222	SWXRTJ074627.1-022551	WISEJ074627.03-022549.3	C	BZB
2FGLJ0756.3-6433	SWXRTJ075624.1-643031	WISEJ075624.60-643030.6	C	BZB
2FGLJ0838.8-2828	SWXRTJ083842.4-282831	WISEJ083842.77-282830.9	C	MIXED
2FGLJ0900.9+6736	SWXRTJ090121.8+673951	WISEJ090121.65+673955.8	C	MIXED
2FGLJ1013.6+3434	SWXRTJ101256.7+343646	WISEJ101256.54+343648.8	C	BZB
2FGLJ1029.5-2022	SWXRTJ102946.9-201808	WISEJ102946.66-201812.6	C	BZQ
2FGLJ1038.2-2423	SWXRTJ103755.0-242543	WISEJ103754.92-242544.5	C	BZQ
2FGLJ1254.2-2203	SWXRTJ125422.8-220414	WISEJ125422.47-220413.6	C	BZB
2FGLJ1347.0-2956	SWXRTJ134707.1-295844	WISEJ134706.89-295842.3	C	BZB
2FGLJ1614.8+4703	SWXRTJ161541.3+471110	WISEJ161541.22+471111.8	C	BZB
2FGLJ1622.8-0314	SWXRTJ162225.3-031439	WISEJ162225.35-031439.6	C	BZQ
2FGLJ1627.8+3219	SWXRTJ162800.3+322413	WISEJ162800.40+322414.0	C	BZQ
2FGLJ1745.6+0203	SWXRTJ174507.7+015442	WISEJ174507.82+015442.5	A	BZQ
	SWXRTJ174526.8+020532	WISEJ174526.95+020532.7	B	BZB
2FGLJ1904.8-0705	SWXRTJ190444.6-070738	WISEJ190444.57-070740.1	C	MIXED
2FGLJ1924.9-1036	SWXRTJ192501.8-104316	WISEJ192501.63-104316.3	C	BZQ
2FGLJ2021.5+0632	SWXRTJ202155.7+062913	WISEJ202155.45+062913.7	C	BZB

Figure 7. Sample SEDs of γ -ray blazar-like sources listed in Table 5 that have a radio counterpart within their XRT positional error. Symbol description is given in Appendix B.

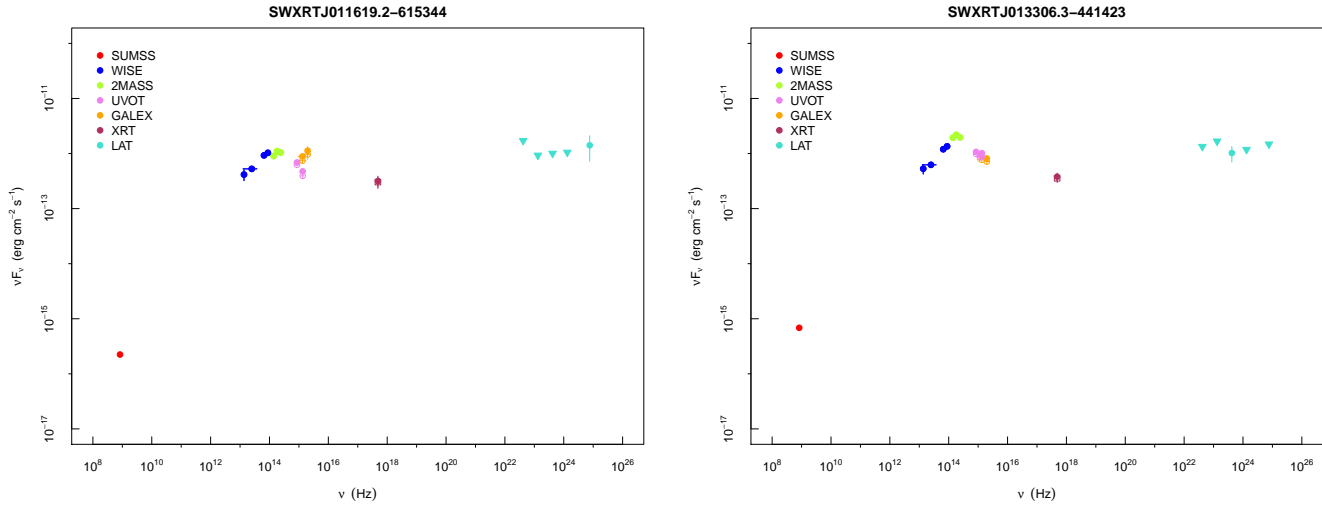


Figure 8. Sample SEDs of γ -ray blazar-like sources listed in Table 5 without a radio counterpart within their XRT positional error. Symbol description is given in Appendix B.

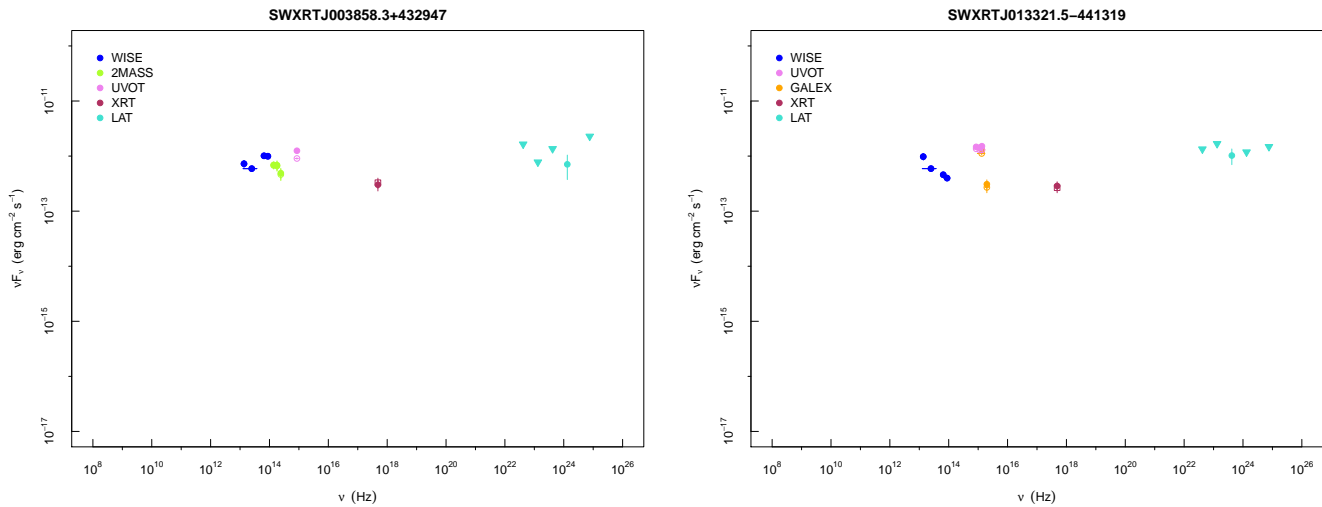


Table 6

XRT-PC counterparts to γ -ray blazar-like sources selected with KDE technique. In boldface we indicate sources with radio counterparts within the positional error listed in Table 1. Column description is given in Appendix B.

NAME 2FGL	NAME XRT	WISE NAME
2FGLJ0031.0+0724	SWXRTJ003119.9+072452	WISEJ003119.70+072453.6
2FGLJ0048.8-6347	SWXRTJ004800.6-634956	WISEJ004800.63-634951.2
2FGLJ0103.8+1324	SWXRTJ010414.0+132427	WISEJ010413.77+132424.5
2FGLJ0200.4-4105	SWXRTJ020020.9-410937	WISEJ020020.94-410935.6
2FGLJ0221.2+2516	SWXRTJ022051.5+250930	WISEJ022051.24+250927.6
2FGLJ0353.2+5653	SWXRTJ035309.5+565429	WISEJ035309.54+565430.8
2FGLJ0420.9-3743	SWXRTJ042025.5-374445	WISEJ042025.09-374445.0
2FGLJ0427.2-6705	SWXRTJ042646.3-665954	WISEJ042646.88-665955.8
2FGLJ0540.1-7554	SWXRTJ054112.1-760249	WISEJ054111.58-760246.1
2FGLJ0737.1-3235	SWXRTJ073739.2-323255	WISEJ073738.91-323256.2
2FGLJ0737.5-8246	SWXRTJ073706.3-824836	WISEJ073706.06-824840.2
2FGLJ0745.5+7910	SWXRTJ074516.0+791310	WISEJ074515.65+791312.3
2FGLJ0746.0-0222	SWXRTJ074554.9-022430	WISEJ074554.80-022430.7
2FGLJ0900.9+6736	SWXRTJ090123.0+672838	WISEJ090122.34+672839.9
2FGLJ1013.6+3434	SWXRTJ101306.5+343460	WISEJ101306.10+343501.6
	SWXRTJ101321.4+343915	WISEJ101321.17+343912.2
2FGLJ1033.5-5032	SWXRTJ103332.0-503531	WISEJ103332.15-503528.8
2FGLJ1038.2-2423	SWXRTJ103748.3-242842	WISEJ103748.10-242845.5
2FGLJ1221.4-0633	SWXRTJ122119.7-063926	WISEJ122119.72-063927.2
	SWXRTJ122154.2-063122	WISEJ122154.19-063124.1
2FGLJ1231.3-5112	SWXRTJ123121.3-511720	WISEJ123121.67-511717.5
2FGLJ1328.5-4728	SWXRTJ132840.4-472749	WISEJ132840.61-472749.2
2FGLJ1517.2+3645	SWXRTJ151752.5+364123	WISEJ151752.12+364125.5
2FGLJ1704.3+1235	SWXRTJ170412.0+123658	WISEJ170412.34+123655.8
2FGLJ1738.9+8716	SWXRTJ174142.4+871445	WISEJ174142.21+871443.6
2FGLJ1748.8+3418	SWXRTJ174925.4+341951	WISEJ174924.98+341951.9
2FGLJ1842.3+2740	SWXRTJ184228.3+273345	WISEJ184228.18+273342.5
2FGLJ2002.8-2150	SWXRTJ200224.2-215113	WISEJ200223.88-215111.6
2FGLJ2034.7-4201	SWXRTJ203451.0-420035	WISEJ203451.08-420038.2
2FGLJ2115.4+1213	SWXRTJ211521.9+121801	WISEJ211522.00+121802.8
2FGLJ2125.0-4632	SWXRTJ212459.7-464006	WISEJ212459.90-464008.4
	SWXRTJ212515.7-463731	WISEJ212515.83-463736.8
2FGLJ2132.5+2605	SWXRTJ213202.1+260306	WISEJ213201.89+260306.1
2FGLJ2228.6-1633	SWXRTJ222830.4-163643	WISEJ222830.19-163642.8
2FGLJ2246.3+1549	SWXRTJ224604.9+154437	WISEJ224604.98+154435.3
2FGLJ2351.6-7558	SWXRTJ235115.2-760017	WISEJ235116.09-760015.5
	SWXRTJ235327.5-760018	WISEJ235328.54-760013.6

Figure 9. Sample SEDs of γ -ray blazar-like sources listed in Table 6 that have a radio counterpart within their XRT positional error. Symbol description is given in Appendix B.

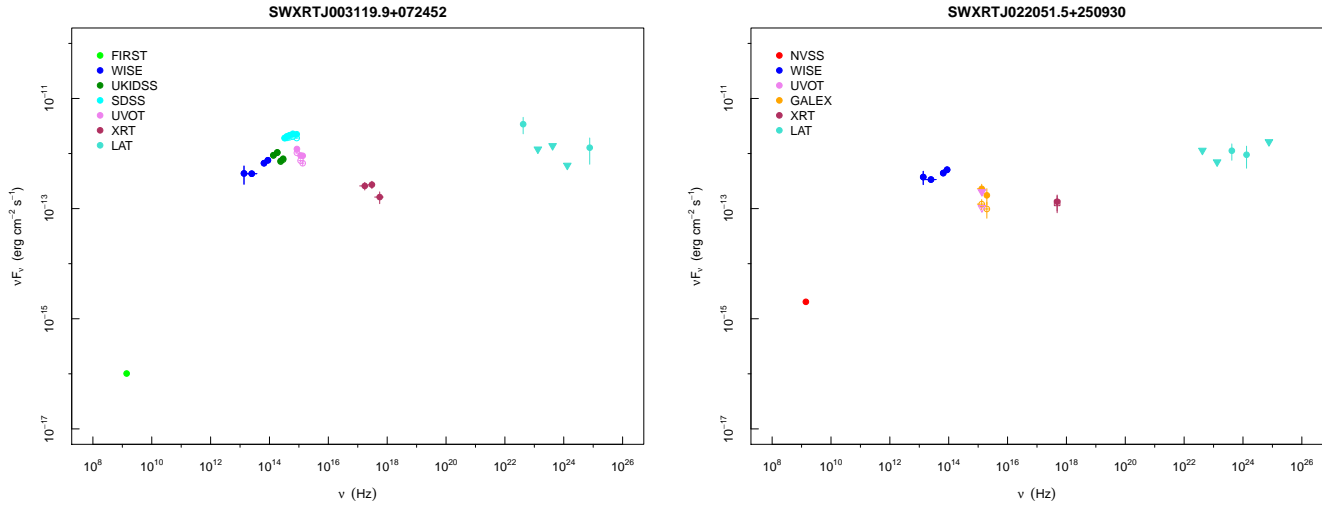


Figure 10. Sample SEDs of γ -ray blazar-like sources listed in Table 6 without a radio counterpart within their XRT positional error. Symbol description is given in Appendix B.

